SUPPORTING INFORMATION

for the manuscript

Optically Induced Avoided Crossing in Graphene

Sören Buchenau, Benjamin Grimm-Lebsanft, and Florian Biebl

Institute of Nanostructure and Solid State Physics,

University of Hamburg, 22761, Germany

Janika Reichstetter and Dirk Manske

Max Planck Institute for Solid State Research, 70569 Stuttgart, Germany

Michael Fechner and Andrea Cavalleri

Max Planck Institute for the Structure and Dynamics of Matter, 22761 Hamburg, Germany

Sonja Herres-Pawlis

Institute of Inorganic Chemistry, RWTH Aachen University, 52074 Aachen, Germany

Michael Rübhausen

Institute of Nanostructure and Solid State Physics,

University of Hamburg, 22761, Germany

(Dated: July 14, 2023)

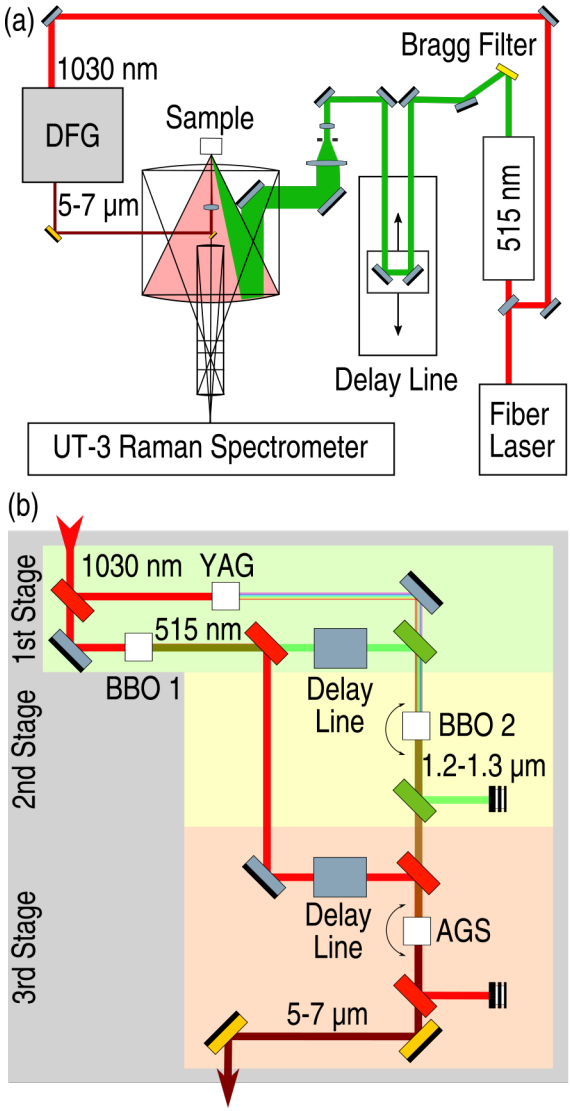

Fig. S1. Schematic of the pump-probe laser setup and the DFG setup.

I. EXPERIMENT

Raman spectroscopy measurements were performed with the UT-3 Raman Spectrometer [1]. The 515 nm second harmonic of a Tangerine fiber laser (France, Amplitude Systemes) was used as the probe beam. The probe beam was widened with a spatial filter and focused on the sample, using the on-axis parabola mirror of the entrance objective, that also collects the scattered light. Energy-dependent measurements shown were taken at 170 kHz, 7 mW probe power and approximately 14 mW pump power. The focus spot sizes of probe and pump beams on the sample were 25 µm and 100 µm, respectively. This leads for the probe (pump)

beam to a pulse energy of 41 (82) nJ and a peak power density of 3.3 (4.2) GW/cm^2. Time-dependent measurements were taken at 350 kHz, 2 mW probe power and approximately 11 mW pump power. This leads for the probe (pump) beam to a pulse energy of 6 (31) nJ and a peak power density of 0.5 (1.6) GW/cm^2. The wavelength of the probe-beam is 515 nm and probe-pulses have a FWHM of approximately 4 ps. The wavelength of the pump beam is varied between 6.0 to 6.5 µm and pump-pulses have a FWHM of approximately 0.5 ps.

The mid-IR pump beam was obtained using a difference frequency generation (DFG) setup as described by the following stages. 1st stage: Super continuum generation in a YAG-crystal and second harmonic generation in a BBO-type-1 crystal with 1030 nm pump. 2nd stage: Optical parametric amplification of the 515 nm pump and super continuum seed in a BBO-type-2 crystal to generate the near-infrared (NIR) beam of 1200-1300 nm. 3rd stage: DFG of 1030 nm pump and NIR seed in an AGS-crystal to generate the mid-IR beam (3-10 µm). The mid-IR beam was focused on the sample using a 40 mm ZnSe-lens. To obtain spatial overlap, a 100 µm pinhole was positioned in the focal point of the entrance objective of the spectrometer. The beam path of the mid-IR beam was optimized for maximum transmission through the pinhole. To ensure temporal overlap, the 515 nm beam was used to induce carriers in a silicon wafer [2] and the transmission of the mid-IR beam was measured as a function of the time delay.

The monolayer and bilayer samples were bought from Matexcel (New York, USA). Both are CVD grown on a 0.5 mm silicon quartz chip with the in-plane dimensions of 1x1 cm^2. The in-plane dimensions are 1x1 cm^2. The multilayer graphene sample was CVD grown on a silicon chip following Ref. [3–5], with the multilayer graphene on a silicon substrate.

II. MONO- AND BILAYER

Figure S2 shows the pumped and unpumped Raman signals on the Anti-Stokes side for (a) the mono- and (b) bilayer graphene sample on the Anti-Stokes side. The energy of the pump pulse is in resonance with the IR-active E_{1u} and the delay is set to zero. No transient Raman signal is observable in the monolayer case. Note that Figure S2 (d) also shows for the bilayer case, an emergence and vanishing of the transient signal within the small bandwidth of the IR phonon.

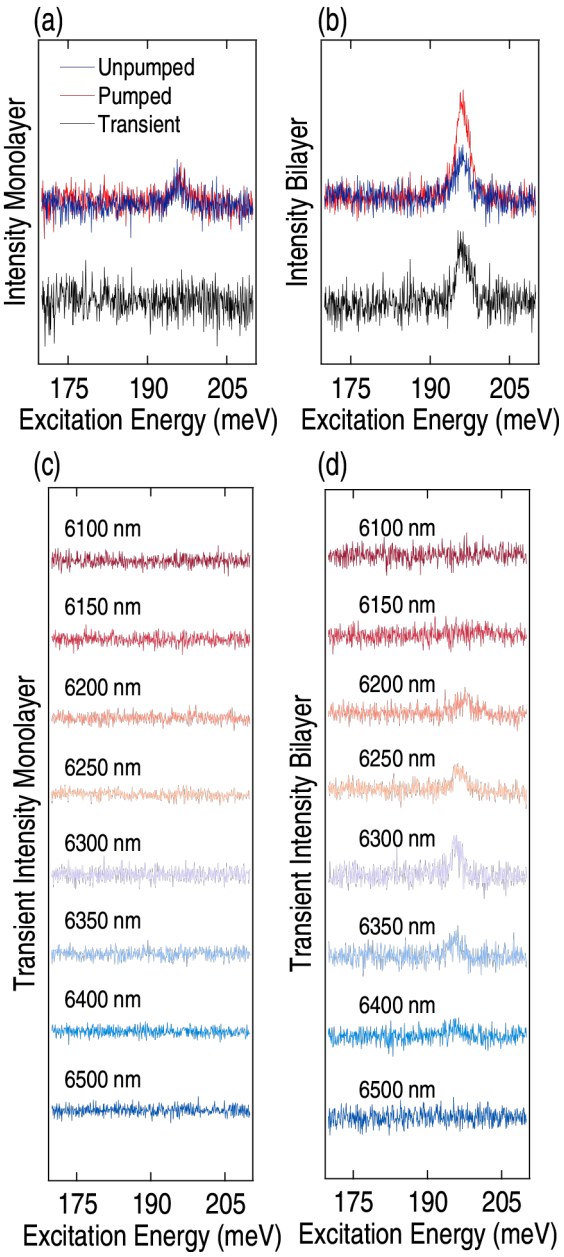

Fig. S2. Pump-energy dependent transient anti-Stokes Raman signal for (a) mono- and (b) bilayer graphene. (c) and (d) show the mid-IR resonant pump-probe experiment for the monolayer and bilayer sample.

III. DELAY DATA

Figure S3 compares the model and the experimental data of the temporal change of the transient shapes, by assuming a dephasing between IR- and Raman-active phonons. This leads to an increase of the ratio between Δ and δ, i.e. real and imaginary parts of the coupled

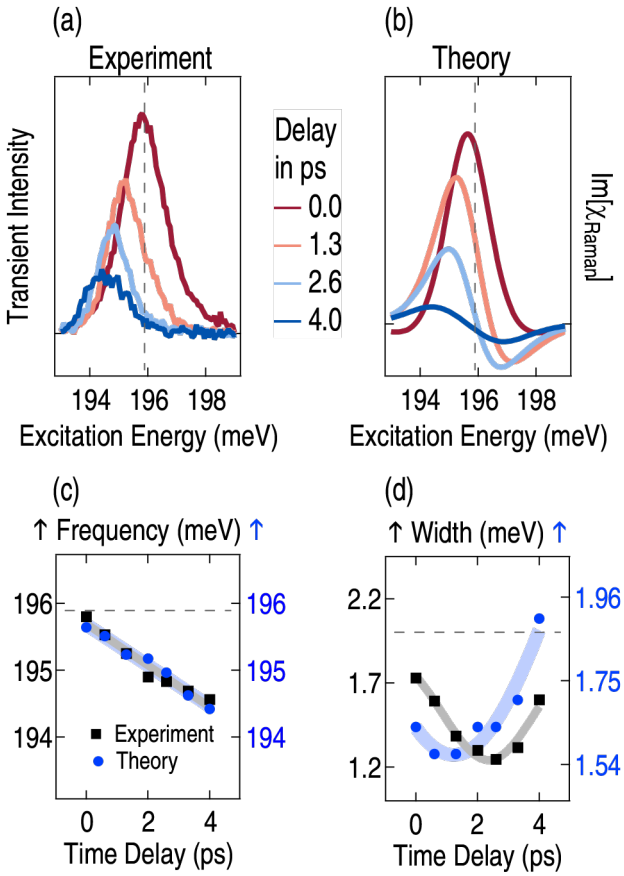

Fig. S 3. Dephasing in experimental and calculated transients. (a) Exemplary time-resolved transient signals. (b) Exemplary calculated transient signals. (c) Frequency tuning of the transient as a function of delay. (d) Change of width as a function of delay. Black squares represent experimental results and blue circles the calculation. Horizontal grey dashed lines indicate the frequency and width of the unpumped Raman phonon and vertical ones the energy of the unpumped IR phonon. Solid grey and blue lines are guides to eye for each parameter.

susceptibilities. After the pump excitation, IR- and Raman-active modes will dephase and accordingly the ratio between Δ and δ will increase. We have used this behavior to model the delay measurements shown in Figure S3 (a), which are well recovered in Figure S3 (b). Indeed, we can also reproduce the observed frequency shift and change in width as shown in Figure S3 (c) and (d) as a function of delay, respectively.

IV. DFT

To estimate the frequency splitting of the IR-active and Raman-active phonon mode, we perform computations in the first-principle framework of density functional theory (DFT). We performed our computations with the Vienna ab-initio simulation package VASP.6.2 [6]. Moreover, for the phonon calculation, we used the Phonopy software package [7]. Our computations utilize pseudopotentials generated within the Projected Augmented Wave (PAW) [8] method. Specifically, we take the following configurated default potential: C $2s^2 2p^2$. We applied the PBEsol [9] approximation for the exchange-correlation potential. As a numerical setting, we used a 27x27x11 or 27x27x1 Monkhorst [10] generated k-point-mesh sampling of the Brillouin zone of graphite or bilayer graphene, respectively. Further we apply a plane-wave energy cutoff of 750 eV. The self-consistent calculations were reiterated until the change in total energy becomes less than 10^{-9} eV.

V. COMPARISON OF ELECTRONIC AND PHONONIC PUMPING

Figure S4 shows a comparison of (a) energy and (b) delay data for the case of phonon-pumping and electronic-pumping in transient spontaneous Raman scattering on multilayer graphene on the anti-Stokes side with a probe beam at 515 nm. In Figure S4 (a) it can be observed that the phononic pumped signal extends over a very narrow range in energies and maps only the IR phonon mode. At a pump energy of 203 meV and 190.7 meV, only approx. 6 meV above and below the maximum resonance, a zero transient can be observed. However, exciting the sample with a 1203.7 meV (1030 nm) pump laser gives a different transient signal. It is clearly observable that on top of the excitation of a transient phonon signal an electronic background transient appears, which is missing for mid-IR pumping. The delay data in Figure S4 (b) also shows different characteristics for each signal. The transients on the left side in panel (b) are taken at 196 meV and are analyzed in the main text. The delay transients on the right side in panel (b), calculated with the same procedure, show a markedly different behavior. Here, the pump laser at 1203.7 meV is in resonance with electronic transitions and shows (I) an increased background up to 4 ps and (II) a significant change in the lineshape between 0 to 4 ps and from 6 ps onwards. These effects can be attributed to the electron-phonon coupling and thermalization effects leading to a shifting

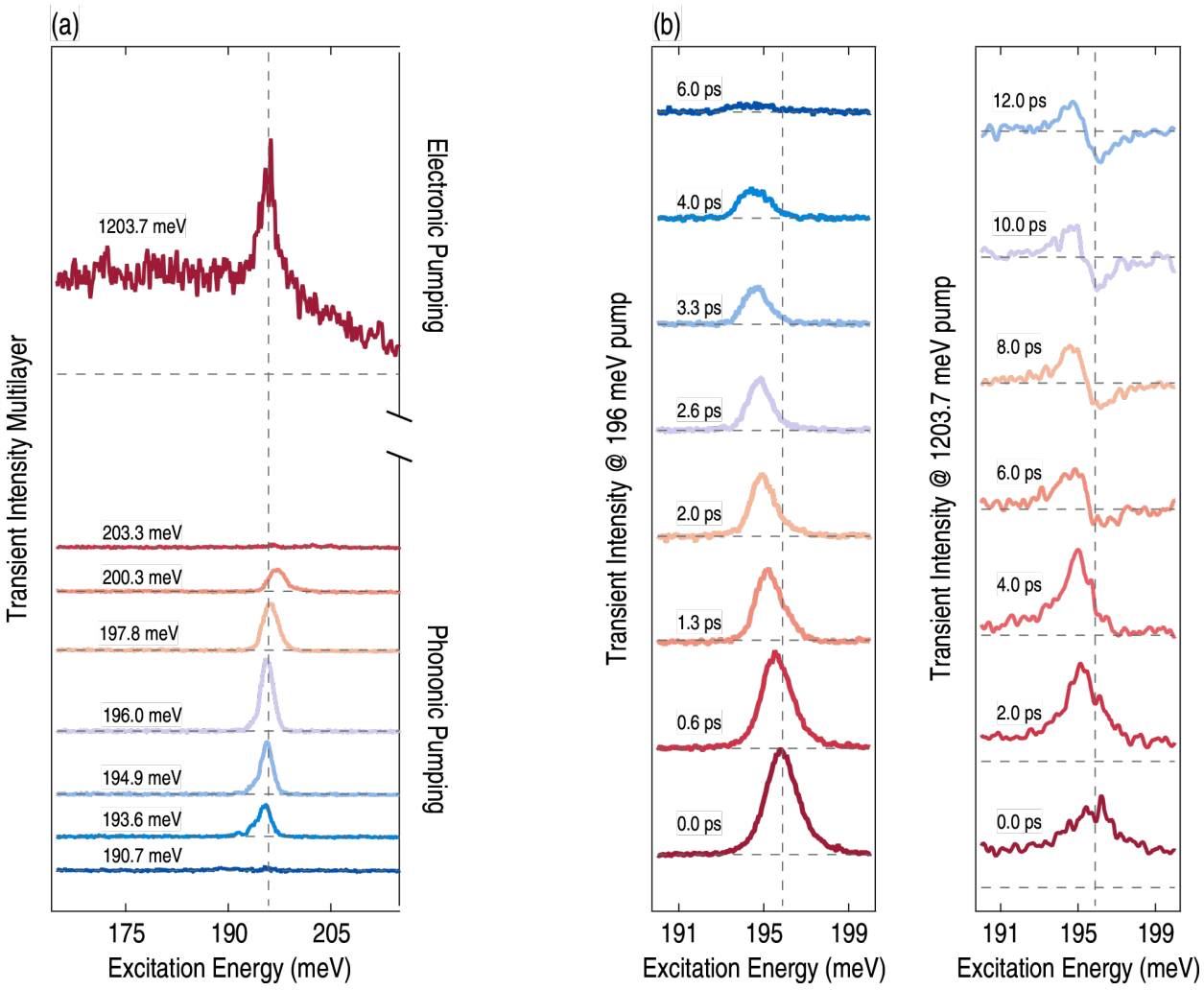

Fig. S 4. Comparison of electronic and phononic pumping in multilayer graphene. (a) shows at zero delay phononic mid-IR pumping in resonance with the G-mode phonon together with an exemplary electronic near-IR pumping at 1203.7 meV. The width of the resonance excitation matched the width of the G-phonon mode. The electronic pumping shows a different transient exhibiting phononic and electronic contributions. (b) shows comparative transient delay scans with the pump energy set to 196 meV (left) and to 1203.7 meV (right), respectively. The transients at 196 meV pump are also shown in Figure S3. Please note that the thermalization of the phonon in (b) is clearly visible by the Fano-like shape of the transients exhibiting a sign change due to the frequency shift of the phonon in the pumped state. Grey dashed lines are zero lines for each transient.

of the phonon mode in the pumped state.

---

[1] B. Schulz, J. Bäckström, D. Budelmann, R. Maeser, M. Rübhausen, M. Klein, E. Schoeffel, A. Mihill, and S. Yoon, Fully reflective deep ultraviolet to near infrared spectrometer and entrance optics for resonance raman spectroscopy, Review of scientific instruments **76**, 097203 (2005).

[2] H. Lo and A. Compaan, Raman measurement of lattice temperature during pulsed laser heating of silicon, Physical Review Letters **44**, 1604 (1980).

[3] H. Baek, H. Kwak, M. S. Song, G. E. Ha, J. Park, Y. Tchoe, J. K. Hyun, H. Y. Park, E. Cheong, and G.-C. Yi, Zno nanotube waveguide arrays on graphene films for local optical excitation on biological cells, APL Materials **5**, 046106 (2017).

[4] Y.-J. Kim, J.-H. Lee, and G.-C. Yi, Vertically aligned zno nanostructures grown on graphene layers, Applied Physics Letters **95**, 213101 (2009).

[5] Y. J. Hong, H. S. Jung, J. Yoo, Y.-J. Kim, C.-H. Lee, M. Kim, and G.-C. Yi, Shape-controlled nanoarchitectures using nanowalls, Advanced Materials **21**, 222 (2009).

[6] G. Kresse and J. Furthmüller, Efficient iterative schemes for ab initio total-energy calculations using a plane-wave basis set, Physical review B **54**, 11169 (1996).

[7] A. Togo and I. Tanaka, First principles phonon calculations in materials science, Scripta Materialia **108**, 1 (2015).

[8] G. Kresse and D. Joubert, From ultrasoft pseudopotentials to the projector augmented-wave method, Physical review b **59**, 1758 (1999).

[9] G. I. Csonka, J. P. Perdew, A. Ruzsinszky, P. H. Philipsen, S. Lebègue, J. Paier, O. A. Vydrov, and J. G. Ángyán, Assessing the performance of recent density functionals for bulk solids, Physical Review B **79**, 155107 (2009).

[10] H. J. Monkhorst and J. D. Pack, Special points for brillouin-zone integrations, Physical review B **13**, 5188 (1976).

[11] L. D. Landau, A theory of energy transfer ii, Phys. Z. Sowjetunion **2**, 19 (1932).

[12] C. Zener, Non-adiabatic crossing of energy levels, Proceedings of the Royal Society of London. Series A, Containing Papers of a Mathematical and Physical Character **137**, 696 (1932).